Effects of Leading-Edge Tubercles on Wing Flutter Speeds

BF Ng[1], TH New[1] and R Palacios[2]

[1] School of Mechanical and Aerospace Engineering, Nanyang Technological University, 50 Nanyang Avenue, Singapore 639798

[2] Department of Aeronautics, 355 Roderic Hill Building, Imperial College, London SW7 2AZ, United Kingdom

E-mail: dthnew@ntu.edu.sg

January 2016

Abstract. The dynamic aeroelastic effects on wings modified with bio-inspired leading-edge (LE) tubercles are examined in this study. We adopt a state-space aeroelastic model via the coupling of unsteady vortex-lattice method and a composite beam to evaluate stability margins as a result of LE tubercles on a generic wing. The unsteady aerodynamics and spanwise mass variations due to LE tubercles have counteracting effects on stability margins with the former having dominant influence. When coupled, flutter speed is observed to be 5% higher, and this is accompanied by close to 6% decrease in reduced frequencies as an indication of lower structural stiffness requirements for wings with LE tubercles. Both tubercle amplitude and wavelength have similar influences over the change in flutter speeds, and such modifications to the leading-edge would have minimal effect on stability margins when concentrated inboard of the wing. Lastly, when used in sweptback wings, LE tubercles are observed to have smaller impacts on stability margins as the sweep angle is increased.

Nomenclature

$\boldsymbol{A}_c$ Aerodynamic influence coefficient matrix

$\boldsymbol{K}$ Discrete stiffness matrix

$\boldsymbol{\mathcal{M}}$ Discrete mass matrix

$\boldsymbol{Q}_{ext}$ External forces

U_f Freestream velocity (flutter)

U_∞ Freestream velocity

a Amplitude of tubercle

c Mean chord length

d Number of bound chordwise panels

k Reduced frequency

$\boldsymbol{w}$ Downwash

$\boldsymbol{x}$ State vector

$\boldsymbol{\Gamma}$ Vortex circulation strength

Λ Sweep angle

$\boldsymbol{\eta}$ Structural degrees-of-freedom

λ Wavelength of tubercle

ω Frequency

Superscript

n Time-step

Subscript

b Bound

r Wing root

t Wing tip

w Wake

Keywords: leading-edge, tubercles, flutter, aeroelasticity, swept-wing, stability

Submitted to: *Bioinspir. Biomim.*

1. Introduction

The motivation to evaluate the influence of leading-edge (LE) protuberances on wing performance is inspired by the works of marine biologists on the morphology of humpback whales [1, 2] (Figure 1). Despite their huge body masses, these sea mammals are particularly agile under water and are capable of performing rolls and loops. Numerous simulations [3, 4, 5, 6] and experiments [7, 8, 9, 10] have been conducted to study the roles these LE tubercles play in the resulting fluid dynamics. In particular, it has been observed that LE tubercles are capable of delaying stall and increase lift in the post-stall regime. In addition, LE tubercles are capable of reducing noise [11, 12]. Driven by these positive findings, there is great interest in applying the concept on aircraft wings, wind and industrial turbines blades [13, 14, 15] to take advantage of improved post-stall aerodynamic performances. However, most of these wings/blades are flexible and an understanding of how LE tubercles affect aeroelastic stability margins is needed. To the best of the authors' knowledge, there has not been an examination on the aeroelastic effects brought about by LE tubercles on wings.

The earliest work investigating the aerodynamic characteristics of LE tubercles was by Watts and Fish [5] using a panel method that showed a 4.8% increase in lift over baseline rectangular wings. Subsequent numerical simulations also confirmed the finding through higher-fidelity numerical methods [16, 17, 18, 19, 20]. These were accompanied by experiments on both full- and semi-span rectangular planforms in either wind [21, 8, 22] or water tunnels [23]. In general, LE tubercles are capable of delaying stall by up to 40% [21], which can be attributed to the delay of flow separation towards the trailing-edge behind tubercle crests. Cavitation occurs in the trough, creating a vortical structure that imposes downwash on the crests to delay stall. Each tubercle can be perceived as a small delta wing having a rounded apex that produces a separated LE vortex on the upper (suction) surface of the tubercle at high angles-of-attack (AoA). This produces a net downwash over each crest and a net upwash over each trough. As a result, localized upwash in the troughs generate higher effective AoA and earlier

Figure 1: Humpback whale (top) and flipper with LE tubercles (bottom). Photographs from [14].

separation as compared to the peaks [16].

LE tubercles are also observed to reduce the point of maximum lift [8] and increase the region of post-stall lift at the expense of reduced lift in the pre-stall regime for semi-span models [7]. On delta wings, tubercles are further observed to foster flow re-attachment and eradicate most of the negative effects of flow separation [13]. The effects of tubercle geometry on aerodynamic performance have also been investigated [9] and it was found that tubercle amplitude has a larger effect on post-stall characteristics as compared to the tubercle wavelength. A larger tubercle amplitude is characterized by a more gradual stall, smaller maximum lift, lower pre-stall lift-slope and higher post-

stall lift. However, it was also found that [24] through optimizing the amplitude and wavelength of the tubercles, pre-stall lift can be maintained with improved post-stall performances.

Flow visualization using dye and tuft have also been performed [9] that showed flow over tubercles remaining attached beyond stall and that separation is concentrated to the leading-edge of troughs. The sensitivity of flow separation to various tubercle configurations was also investigated using hydrofoils [25] at low Reynolds numbers through particle-image velocimetry (PIV) measurements [26, 27, 28]. Apart from these studies that mainly focused on steady flows, Ozen and Rockwell [23] provided flow visualizations of a flapping rectangular wing with LE tubercles, demonstrating passive control of flow structure inboard of the wing. These studies, however, have all treated the lifting surfaces as rigid bodies and no fluid-structure interactions were considered. In particular, detailed aeroelastic analysis is currently lacking and would be necessary if LE tubercles were to be applied to aircraft, energy and industrial applications [29, 30, 31].

In this study, we aim to investigate aeroelastic stability margins due to the presence of LE tubercles on rectangular wings. This will shed light on the design of LE tubercles such that improved post-stall performance can be achieved with an understanding of how pre-stall stability is affected. Particularly, in the pre-stall regime, instability (flutter) on wings is likely due to slenderness and the rear positioning of the centre-of-gravity. Also, it has been shown that the lift slope at low AoA (below 12°) for configurations with LE tubercles is within 5% of linear aerodynamic theory [21]. Therefore, we approach the problem by adopting a state-space aeroelastic model coupling the unsteady vortex-lattice method (UVLM) with a composite beam. The state matrix is then used to evaluate stability margins with a model of a typical aeroelastic wing. A brief introduction of the aeroelastic formulation will first be presented in Section 2, which is written in a state-space form to allow eigenvalue analysis and is numerically verified in Section 3.1. Subsequently, the stability of a flexible wing with LE tubercles is investigated in Section 3.2, with suggestions on tubercle placement for minimal impact on stability.

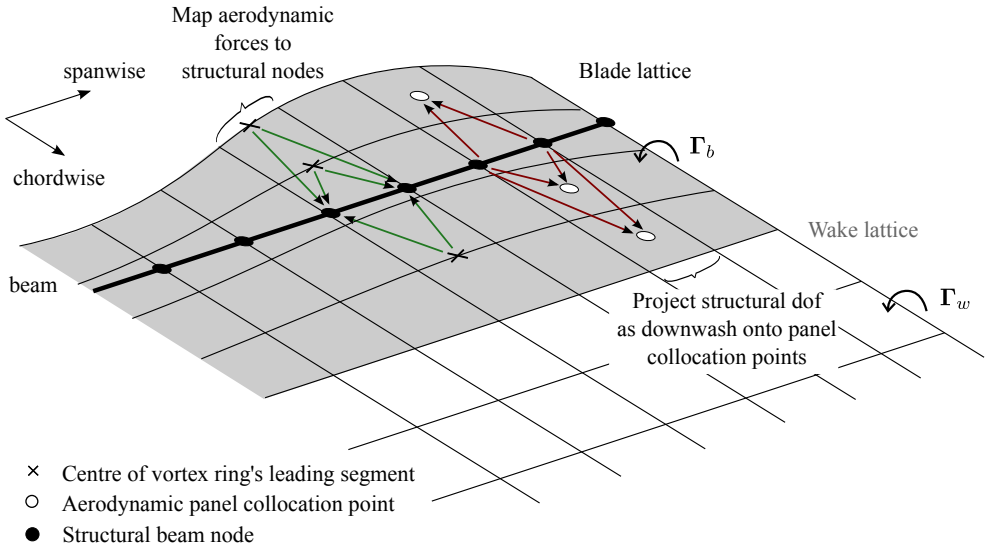

Figure 2: Coupling between beam and vortex panels.

Swept wings with LE tubercles are then considered in Section 3.3 to investigate the effects of different tubercle configurations in increased spanwise flow conditions on stability margins.

2. Aeroelastic Formulation

The aeroelastic description is based on the integrated framework for the Simulation of High Aspect Ratio Planes (SHARP), which has been previously developed to study the dynamics of flexible aircraft [32] and wind turbines [33, 34] for linear stability analysis, time-marching simulations and control synthesis.

A composite beam is used to represent the dynamics of the flexible structure as shown in Figure 2. The structural description is capable of accounting for large static and transient deformations, and an appropriate cross-sectional methodology is implemented to reduce three-dimensional structures to a one-dimensional representation. The nodal displacements and rotations from the finite element discretization is represented by $\boldsymbol{\eta}$. For stability analysis, the structural equations of motion (EoM) are linearized about a steady-state equilibrium $\boldsymbol{\eta}_0$. The incremental form of the beam EoM (without rigid-

body motion) can be expressed as

$$\boldsymbol{\mathcal{M}}\left(\boldsymbol{\eta}_0\right)\Delta\ddot{\boldsymbol{\eta}} + \boldsymbol{K}\left(\boldsymbol{\eta}_0\right)\Delta\boldsymbol{\eta} = \Delta\boldsymbol{Q}_{ext}, \tag{1}$$

where $\boldsymbol{\mathcal{M}}$ and $\boldsymbol{K}$ are the mass and stiffness matrices, respectively, and structural damping is not included as it is assumed to be small as compared to aerodynamic damping. External forces are given by $\boldsymbol{Q}_{ext}$, which can be used to represent aerodynamic forces.

The unsteady aerodynamics are modeled using the discrete-time UVLM [35] with a planar wake to capture the non-stationary aerodynamics in low-speed and high Reynolds number attached-flow conditions. In the UVLM, vortex rings are used as the fundamental solutions and are located in lattices to represent the lifting surface, as shown in Figure 2. Neumann boundary conditions are subsequently imposed for zero normal velocity at each collocation point due to vortices and motion of the lifting surface. This is given by

$$\boldsymbol{A}_{c,b}\boldsymbol{\Gamma}_b^{n+1} + \boldsymbol{A}_{c,w}\boldsymbol{\Gamma}_w^{n+1} + \boldsymbol{w}^{n+1} = \boldsymbol{0}\,, \tag{2}$$

where $\boldsymbol{\Gamma}_b$ and $\boldsymbol{\Gamma}_w$ are the bound and wake vortex circulations, respectively. The influence coefficients $\boldsymbol{A}_{c,b}$ and $\boldsymbol{A}_{c,w}$ are resolved using the Biot-Savart law, relating the induced normal velocities at collocation points to the bound and wake vortices, respectively. The downwash at collocation points $\boldsymbol{w} = \boldsymbol{w}_{\boldsymbol{\eta}} + \boldsymbol{w}_{\delta}$ is generated by the motion of the lifting surface (mapped from structural deformations) and external disturbances (e.g., gust profiles). Each vortex ring in the wake that is shed from the trailing edge has a chordwise length of $U_\infty \times \Delta t$, where U_∞ is the freestream velocity. The time-step Δt is determined by the UVLM discretization, which can be represented as $\Delta t = c/(U_\infty d)$, where c is the mean chord length and d is the number of bound chordwise panels. To facilitate a linear time-invariant (LTI) state-space description of the UVLM, the wake is frozen in either a planar or rolled-up configuration. In this study, a planar wake is sought and it has been shown that the computation of aerodynamic loads (used here for the fluid-structure coupling) displayed little differences with free-wake models [32].

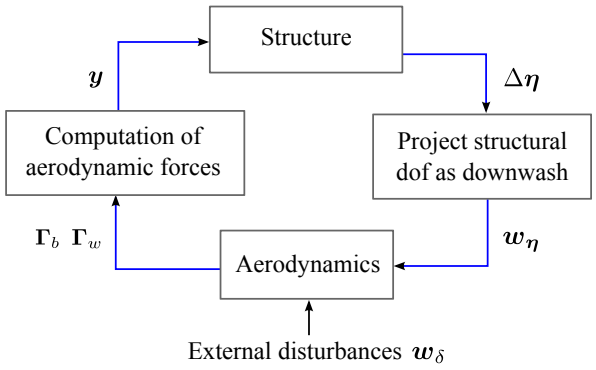

Figure 3: Block diagram of fluid-structure coupling.

The structural EoM in continuous time are discretized through the Newmark-β method and subsequently coupled with the discrete-time UVLM, arriving at the complete aeroelastic system in state-space representation. As shown in Figure 2, structural degrees-of-freedom are mapped onto panel collocation points as downwash and in turn, the computed aerodynamic forces are mapped to the structural nodes. A block diagram of the fluid-structure coupling illustrating the flow of parameters is shown in Figure 3 and further details can be found in [36]. The resulting coupled LTI EoM characterizing the full aeroelastic system is

$$\begin{aligned} \boldsymbol{x}^{n+1} &= \boldsymbol{A}\boldsymbol{x}^n + \boldsymbol{B}\boldsymbol{w}\,, \\ \boldsymbol{y}^n &= \boldsymbol{C}\boldsymbol{x}^n + \boldsymbol{D}\boldsymbol{w}\,, \end{aligned} \tag{3}$$

where the state vector defining the aeroelastic system is $\boldsymbol{x}^T = \left[\Delta\boldsymbol{\Gamma}_b^T \ \Delta\boldsymbol{\Gamma}_w^T \ |\Delta\boldsymbol{\eta}^T \ \Delta\dot{\boldsymbol{\eta}}^T\right]$, comprising the aerodynamics and structural states. The output $\boldsymbol{y}$ contains the lift on each panel and moment about the elastic axis, and are computed from the pressure distribution across each panel using the unsteady Bernoulli equation [35]. The eigenvalues of the state matrix $\boldsymbol{A}$ define the stability of the system.

3. Numerical Results

The aeroelastic formulation is first numerically verified against the Goland wing [37], which is a generic lifting surface commonly used for benchmarking numerical solutions. It will then be used to model LE tubercles on its baseline and sweptback configurations.

Table 1: Goland wing properties [38].

Chord (m)	1.83
Semi-span (m)	6.10
Elastic axis from LE (m)	0.33·c
Centre of gravity from LE (m)	0.43·c
Mass per unit length (kg/m)	35.7
Moment of inertia (kg·m)	8.64
Torsional stiffness (N·m^2)	0.99×10^6
Bending stiffness (N·m^2)	9.77×10^6

3.1. Numerical Verification

The Goland wing is a rectangular cantilever wing with a semi-span of 6.096 m and chord of 1.829 m. The structural characteristics can be found in Table 1. The flutter speed (U_f) for the Goland wing in straight flight at sea-level has been reported to be 163.5 m/s in Wang *et al* [39]. Using the aeroelastic formulation and checking for stability, U_f obtained from eigenvalue analysis is 160 m/s using 80 chordwise and 20 spanwise panels. The frequency of oscillation at flutter (ω_f) is around 11.2 Hz and the mode of flutter is comprised of the first bending and first torsional modes as illustrated in Figure 4.

3.2. Baseline Configuration

As the UVLM requires a structured discretization, chordwise dimensions of the panels are equally distributed despite varying chord lengths due to tubercle peaks and troughs, shown in Figure 5. As each bound and wake circulation in the UVLM discretization represents a variable, the coupled aeroelastic EoM contain a large number of states. Through a convergence study, a total of 80 chordwise and 24 spanwise panels with 5 wake chords are used for the simulations. This amounts to over 12,000 states, including structural degrees-of-freedom. Each simulation run from the assembly of coupled state matrix to the eigenvalue analysis for each velocity, took approximately 30 minutes on a single processor machine.

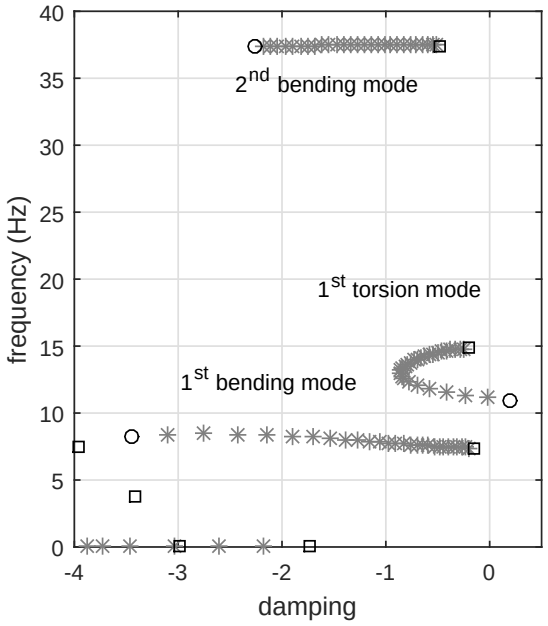

Figure 4: Root locus for increasing velocity from 20 m/s (square) to 165 m/s (circle) in increments of 5 m/s for the Goland wing.

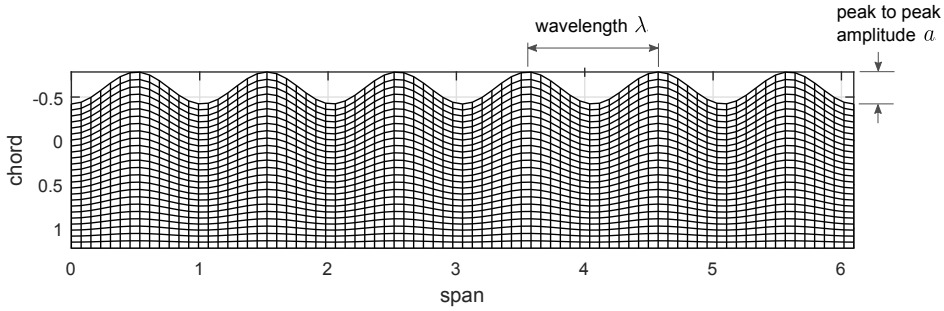

Figure 5: Discretization on the modified Goland wing with LE tubercles of $\lambda = 0.56$·c, $a = 0.2$·c.

3.2.1. Unsteady Aerodynamics and Spanwise Variation of Structural Properties To understand the contribution of LE tubercles to the unsteady aerodynamics, the coefficient of lift with and without LE tubercles (of wavelength $\lambda = 0.56$·c and amplitude $a = 0.2$·c, where c is the chord) undergoing harmonic motions (of $\pm 10^\circ$ AoA) are plotted in Figure 6. The reduced frequencies of 0.1 and 0.4 are shown corresponding to moderate and highly unsteady flow conditions, respectively. The latter condition of $k = 0.4$ is close to the reduced frequency at flutter. With LE tubercles, the quasi-steady lift coefficient is reduced by about 1.5% to 2.0%. However, the unsteady aerodynamics are little affected

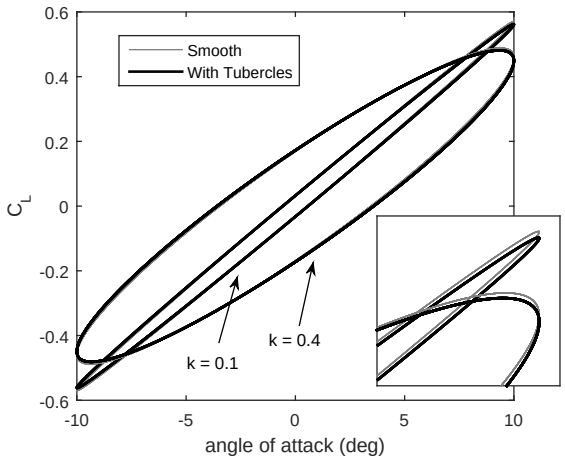

Figure 6: Coefficient of lift for Goland wing with and without LE tubercles (wavelength 0.56·c and amplitude 0.2·c) undergoing harmonic motion (±10° AoA) at reduced frequencies of $k = 0.1$ and $k = 0.4$.

by the LE tubercles. The reduction in quasi-steady lift has the effect of increasing stability margins (flutter speed).

In order to modify a wing with LE tubercles, material has to be added and removed from the baseline configuration to accommodate for the tubercle peaks and troughs, respectively. As a result, sectional mass will vary spanwise in accordance to the location of the tubercles. This also affects the location of the centre-of-gravity (c.g.) and torsional inertia of the structure. Assuming uniform mass distribution on the Goland wing, the torsional inertia, mass and c.g. locations are varied by the ratio of the sectional chord at various spanwise locations with and without LE tubercles. In addition, it is assumed that the load bearing structure of the wing is unaffected such that stiffness values remains unchanged.

The resulting first bending and torsional frequencies for varying tubercle amplitude (of constant wavelength of 0.56·c corresponding to 6 tubercles) and varying tubercle wavelength (of constant amplitude of 0.2·c) are shown in Figure 7a and Figure 7b, respectively. The plots compare between uniform structural properties, spanwise structural variation of torsional inertia alone and that of varying torsional inertia, mass and c.g. positions. As the tubercle amplitude is increased to 0.3·c, the first

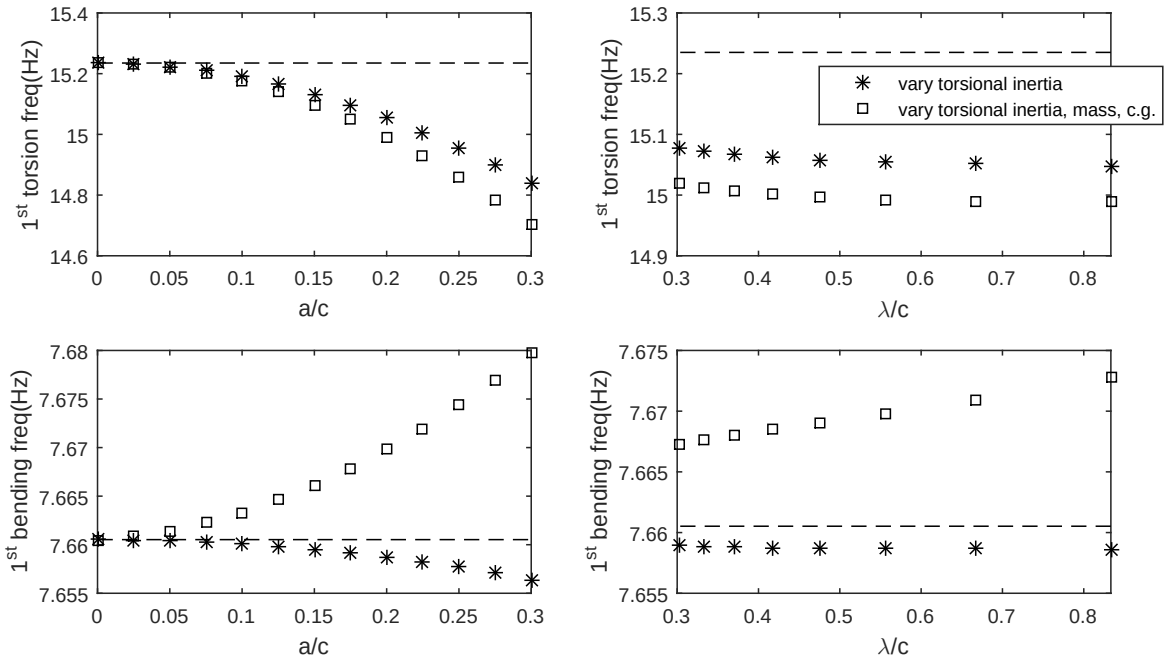

(a) Varying tubercle amplitude with uniform wavelength of 0.56·c.

(b) Varying tubercle wavelength with uniform amplitude of 0.2·c.

Figure 7: Effect of varying tubercle amplitude and wavelength on the first bending and torsional frequencies of the Goland wing. Comparing between spanwise structural variation of torsional inertia alone (∗) and varying torsional inertia, mass and c.g. positions (□). Dotted lines correspond to the natural frequencies of the baseline Goland wing configuration.

torsional frequency is reduced by around 2.5%, which can have the effect of reducing stability margins. This reduction in torsional frequency is predominantly contributed by the spanwise variation in torsional inertia. Spanwise variation of mass and c.g. locations further reduces the torsional frequency by around 0.2%. The changes in first bending frequency is only marginal. When the number of tubercles is varied (from wavelength 0.83·c to 0.33·c corresponding to increasing number of tubercles from 4 to 10), the changes in the first bending and torsional frequencies are small. However, as the number of tubercles is increased (reducing λ/c), the frequencies tends toward the baseline configuration due to increasing spanwise averaging of structural properties.

3.2.2. Variation of Tubercle Geometry on Stability Margins. Separately, the unsteady aerodynamics has the potential of increasing stability margins due to reduced lift with LE tubercles and the structures are seen to reduce torsional frequency such that stability margins could be reduced. It is vital at this stage to investigate how these two counteracting mechanisms affect aeroelastic stability margins when combined.

Two cases of structural configurations are considered here - uniform inertia properties and varying inertia properties such that the torsional inertia, mass and c.g. are varied spanwise to account for the LE tubercles. The effects of LE tubercles with various amplitudes and wavelengths on flutter speeds are shown in Figure 8a and Figure 8b, respectively. In these plots, the vertical axes denote the percentage change in flutter speed due to LE tubercles, taken with respect to the flutter speed of the baseline configuration without LE tubercles.

In Figure 8a, as the tubercle amplitude is increased to 0.2·c while maintaining an uniform wavelength of 0.56·c, we observe an increase in flutter speeds of up to 7% for uniform inertia properties. This is accompanied with a slight increase in the frequency at flutter. With spanwise varying inertia properties, the percentage increase in flutter speed is smaller at around 5.5% due to the lower torsional frequencies as observed in Figure 7a. The reduction in torsional frequency is also translated to a decrease in frequency at flutter as shown in Figure 8c.

When tubercle wavelength is reduced from 0.83·c to 0.33·c (i.e. number of tubercles increased from four to ten) with uniform amplitude of 0.2·c, flutter speeds are increased by up to 5.5% for uniform inertia properties and up to 5% for varying inertia properties (Figure 8b). In the case of frequency at flutter in Figure 8d, the frequencies are higher in the case of uniform inertia properties but lower when inertia variations are considered.

The combination of frequency and flutter speed allows us to quantify the stiffness criteria through reduced frequencies [40, 41]. The reduced frequency, given by $k = \omega_f c/(2U_f)$, where c is the mean chord, provides a stiffness criteria for the lower limit to the ratio between stiffness and flow velocity, below which will result in flutter [42, 43].

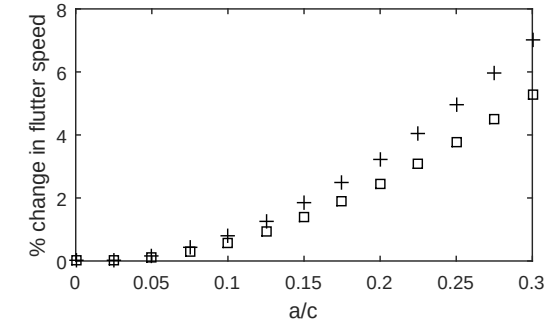

(a) Flutter speed - Varying tubercle amplitude.

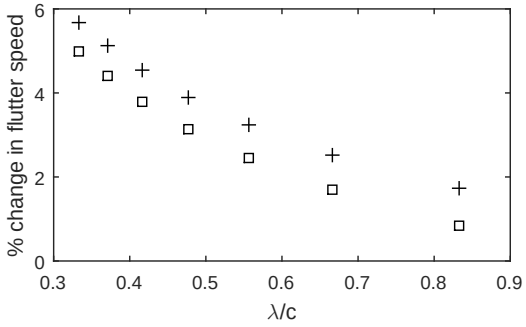

(b) Flutter speed - Varying tubercle wavelength.

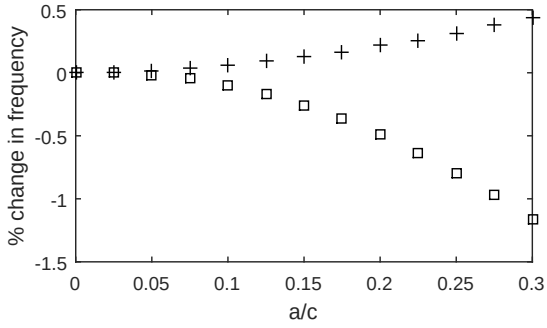

(c) Frequency - Varying tubercle amplitude.

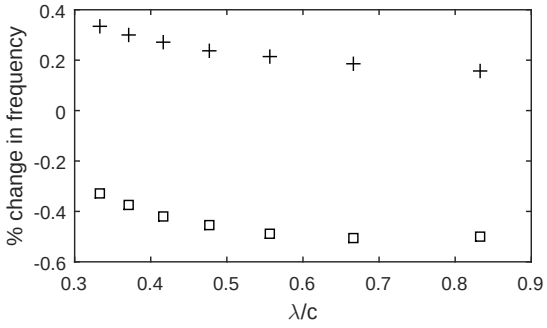

(d) Frequency - Varying tubercle wavelength.

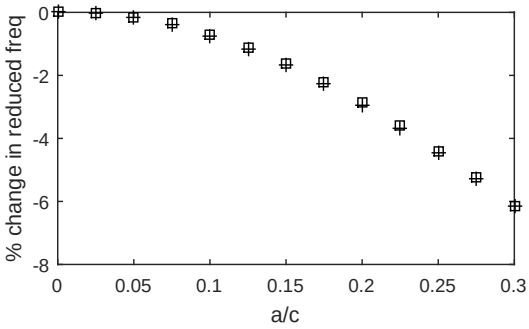

(e) Reduced frequency - Varying tubercle amplitude.

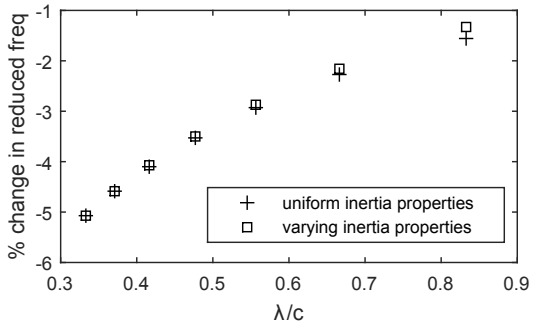

(f) Reduced frequency - Varying tubercle wavelength.

Figure 8: Effect of varying tubercle amplitude (with uniform wavelength of 0.56·c) and tubercle wavelength (with uniform amplitude of 0.2·c) on percentage change in the flutter speed, frequency and reduced frequency. Shown with uniform (+) and spanwise varying (□) inertia properties.

Without LE tubercles, the reduced frequency of the Goland wing at flutter is around 0.418. With increasing tubercle amplitude and wavelength, reduced frequencies are reduced by 6% and 5% in Figure 8e and Figure 8f, respectively. The values for uniform and varying inertia properties overlap.

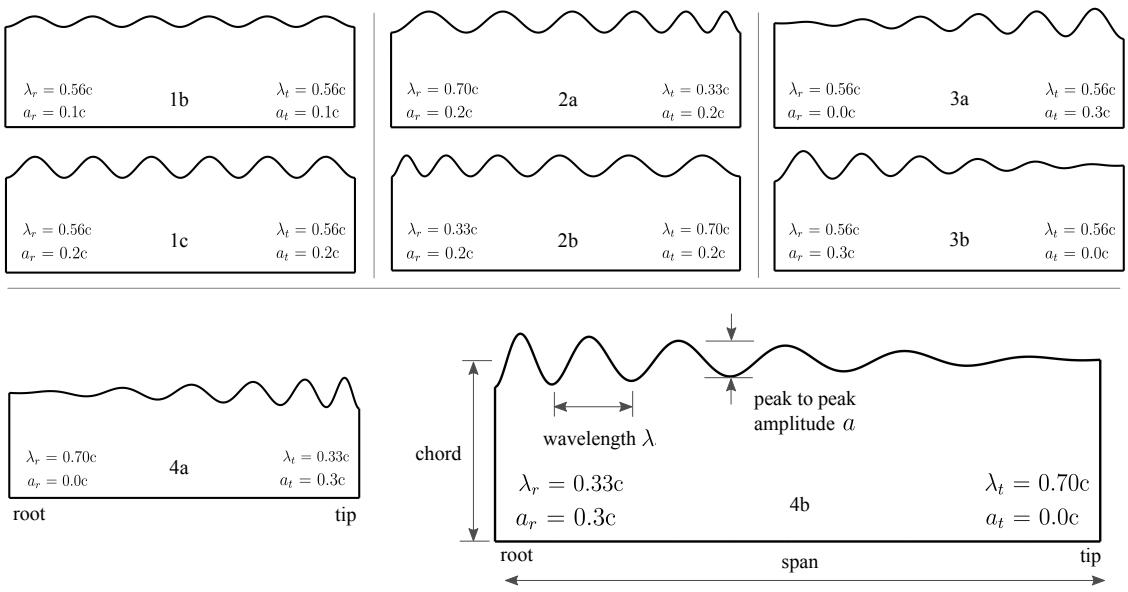

Figure 9: Configurations for spanwise variation of LE tubercle geometry.

Table 2: Percentage change in flutter speed for linear spanwise variation of tubercle amplitudes and wavelengths. All configurations have six LE tubercles and geometries are shown in Figure 9. The abbreviations are: a_r amplitude at root, a_t amplitude at tip, λ_r wavelength at root, λ_t wavelength at tip, c mean chord.

Config.	a_r/c	a_t/c	λ_r/c	λ_t/c	**% change in U_f**
1a (baseline)	0.0	0.0	0.0	0.0	-
1b	0.1	0.1	0.56	0.56	0.59
1c	0.2	0.2	0.56	0.56	2.44
2a	0.2	0.2	0.70	0.33	2.94
2b	0.2	0.2	0.33	0.70	1.65
3a	0.0	0.3	0.56	0.56	2.31
3b	0.3	0.0	0.56	0.56	0.99
4a	0.0	0.3	0.70	0.33	3.29
4b	0.3	0.0	0.33	0.70	0.88

3.2.3. Spanwise variation of Tubercle Geometry. Tubercle amplitudes and wavelengths could also vary spanwise to take advantage of localized effects. Table 2 shows the percentage change in flutter speeds when tubercle amplitudes and wavelengths are varied spanwise on the Goland wing (including variation of inertia properties). Their corresponding geometries are shown in Figure 9. Configurations 1a, 1b and 1c are

baseline cases without and with LE tubercle of uniform amplitude and wavelength. In configuration 2a, the tubercle wavelength is varied from 0.70·c to 0.33·c from root to tip (i.e. more tubercles towards the wing tip and maintaining a total of six tubercles) while keeping a uniform amplitude of 0.2·c. The percentage increase in flutter speed is at 2.94%. Conversely, with more tubercles towards the root in configuration 2b, the percentage increase in flutter speed is lower at 1.65%. Varying tubercle amplitude from root to tip while keeping a uniform wavelength in configurations 3a and 3b, the increase in flutter speed is higher when tubercle amplitudes are larger towards the tip.

When both a larger amplitude and a smaller wavelength are concentrated towards the tip in configuration 4a, the increase in flutter speed could be as high as 3.29%. On the other hand in configuration 4b, when tubercles are concentrated towards the root, the effect on flutter speed is minimal at only 0.88%. From an aeroelastic perspective, the wing root experiences smaller displacements/rotations as compared to the tip and hence the aerodynamic effects due to LE tubercles clustered around the root on stability margins are smaller than when they are located near the tip.

3.3. Sweptback Configuration

Typical configurations of lifting surfaces have certain amount of sweep and on the humpback whales, the fins are also tapered. As such, the effects of LE tubercles on stability margins in spanwise flow can be further understood from swept configurations of the Goland wing. A typical configuration of the swept wing [44] is shown in Figure 10a where the chord is defined perpendicular to the leading-edge. In this investigation, we consider two swept models - shear-swept and constant length-to-chord ratio [44]. In the shear-swept model (Figure 10b), the wing is swept back such that cross-sections remain parallel to the freestream. The wing area, span and hence aspect ratio are unchanged through sweep and are compensated by a reduction in chord. In the constant length-to-chord model, the wing is rotated with the root and tip modified to align parallel to the freestream. The wing area, chord and length are unchanged.

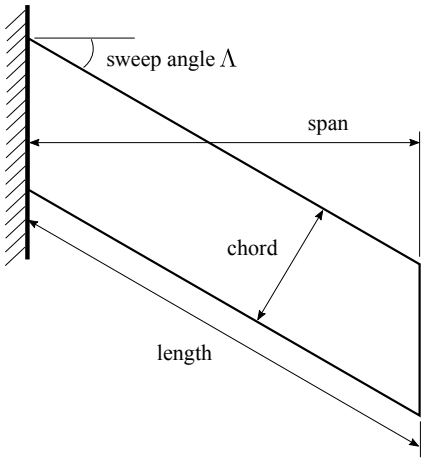

(a) Representation of a swept wing.

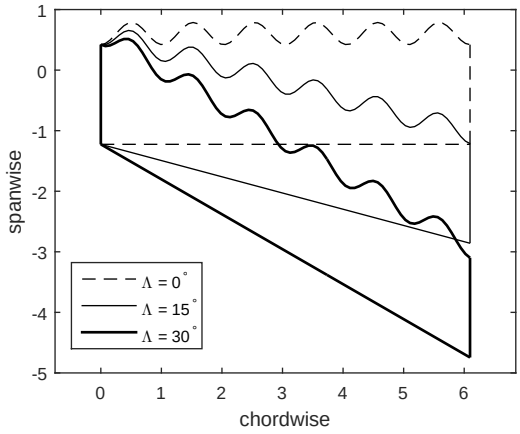

(b) Shear-swept wings with constant aspect ratio.

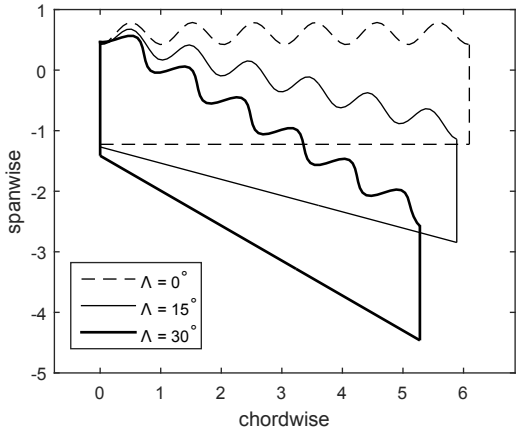

(c) Swept wings with constant length-to-chord ratio.

Figure 10: Swept wing configurations.

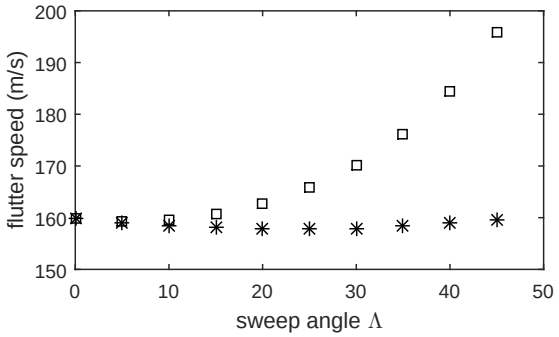

(a) Flutter speed.

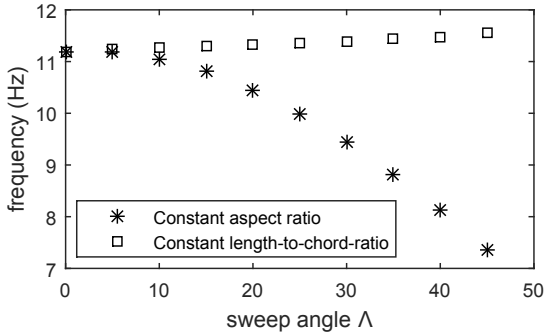

(b) Frequency.

Figure 11: Effect of wing sweep on flutter speeds and frequencies of the baseline model without LE tubercles. Comparing wing swept with constant aspect ratio (∗) and constant length-to-chord-ratio (□).

The influence on flutter speeds due to sweep through shear (constant aspect ratio) and constant length-to-chord ratio are shown in Figure 11a. In the shear-swept model, flutter speed exhibits a gentle U-shaped trend as sweep angle is increased. The flutter speed initially decreases due to longer wing length, which is eventually overcome by the increased spanwise flow that stabilises the system. On the other hand, in constant length-to-chord swept wings, flutter speeds falls slightly for 5° to 10° sweep and then increases by about 20% at 45° sweep due to the shorter wing span and increased spanwise flow. This trend coincides with the classical results of Refs [45, 46].

The mode of flutter for both sweep models comprise of the first bending and first torsional modes. With increasing sweep angle up to 45°, the frequency at flutter is reduced by a maximum of 34% and increased by 4% for the shear-swept and constant length-to-chord swept wings, as shown in Figure 11b. In the former, the reduction in flutter frequency is due to longer wing length (longer beam) as the wing is swept through shear whereas in the latter, the increase in flutter frequency is due primarily to aerodynamic spanwise effects as the wing length is kept constant.

3.3.1. Varying Tubercle Amplitude on Swept Models. In modifying the swept wings to accommodate LE tubercles, the amplitude and wavelength are parameterized with reference to the chord perpendicular to the leading-edge. The structural properties including mass, torsional inertia and c.g location are also varied spanwise. As sweep angle is increased in both the shear-swept and constant length-to-chord ratio models, LE tubercles of larger amplitudes (while keeping a constant number of six tubercles) have lesser impact on flutter speeds as shown in Figure 12a and Figure 12c, respectively. At 15° sweep, the maximum increase in flutter speed is around 5% compared to 3.5% for 45° sweep for both swept configurations. Note that percentages are taken against the respective swept configurations without LE tubercles. The reduced effect on flutter speed as sweep angle is increased can be attributed to the spanwise effects of LE tubercles. In the shear-swept wing, the longer wing span increases tubercle wavelength

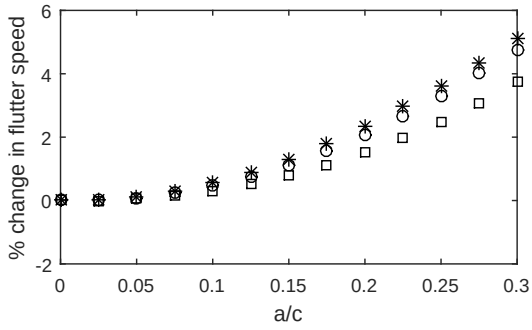

(a) Shear-swept with constant aspect ratio. Varying tubercle amplitude.

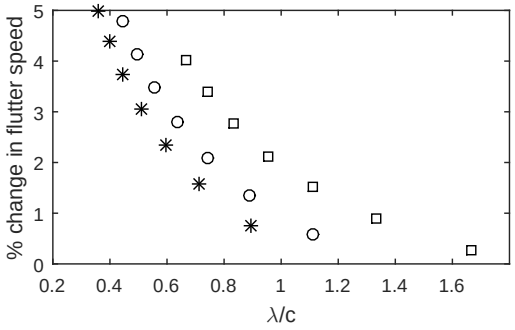

(b) Shear-swept with constant aspect ratio. Varying tubercle wavelength.

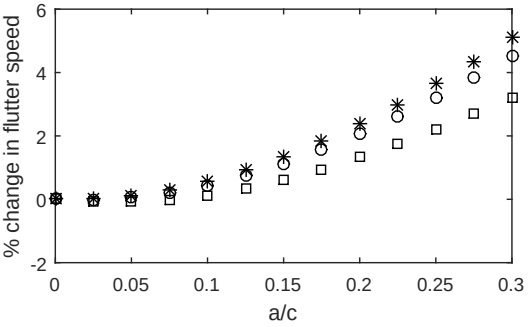

(c) Swept with constant length-to-chord ratio. Varying tubercle amplitude.

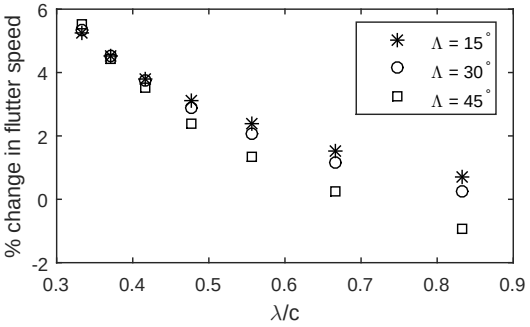

(d) Swept with constant length-to-chord ratio. Varying tubercle wavelength.

Figure 12: Effect of varying tubercle amplitude (with six tubercles) and tubercle wavelength (with amplitude 0.2·c) on flutter speeds for different swept models and sweep angles - 15° (∗), 30° (○) and 45° (□).

for the same number of LE tubercles, thus reducing the effectiveness of LE tubercles. In the constant length-to-chord ratio swept wing, the effective tubercle amplitude with respect to the swept chord (parallel to freestream) is smaller as sweep angle is increased, thus reducing the effects of LE tubercles on flutter speeds. The mode of flutter with increased tubercle amplitude for various sweep angles is still dominated by the first bending and first torsional modes.

3.3.2. Varying Tubercle Wavelength on Swept Models. When the number of LE tubercles is increased (while keeping a constant amplitude of 0.2·c), flutter speeds are increased for both the shear-swept and constant length-to-chord swept wings. In the former, with flutter speeds plotted in Figure 12b, the effects of a larger number of

LE tubercles on flutter are smaller as the sweep angle is increased. At 15° sweep, the maximum increase in flutter speed is around 5% compared to 4% for 45° sweep. This is attributed to a larger tubercle wavelength from longer wing length. Note that the wavelength intervals λ/c differ among the shear-swept angles due to varying wing length but they indicate an increase in number of LE tubercles from four to ten. In the wing swept through constant length-to-chord ratio in Figure 12d, as the number of LE tubercles is increased, there is an increasingly similar influence on flutter speeds as the sweep angle is increased. With only four LE tubercles (wavelength of 0.83·c), the 45° swept wing has a smaller influence on flutter speed compared to a 15° swept wing. However, the differences are reduced as the number of tubercles is increased. The mode of flutter remains as a coupling between the first bending and torsional modes.

4. Conclusion

Bio-inspired engineering may provide ideas to improve existing aerodynamics but thorough analysis is still required before they can be applied to flight or industrial uses. We have shown that leading-edge tubercles increase stability margins for a given amount of lift, offering an additional advantage to stall delays. The aerodynamics and spanwise inertia variations with LE tubercles have counteracting effects on stability margins, with the former increasing stability margins due to reduced lift and the latter reducing stability margins from lower torsional frequencies. When coupled in an aeroelastic description, stability margins are dominated by the aerodynamics where flutter speeds are increased by up to 5% with six LE tubercles of amplitude 0.2·c. The mode of flutter is unchanged through LE tubercles and consist of a coupling between the first bending and first torsional modes. Both tubercle amplitude and wavelength have similar influence over the flutter speed and wings modified with LE tubercles can benefit from lower structural stiffnesses to maintain the nominal stability margin. It is also shown that LE tubercles concentrated towards the wing root have a smaller effect on stability margins. When placed on swept wings, LE tubercles have smaller effects on flutter speeds as

the sweep angle is increased. The current investigation have illustrated LE tubercles on a typical wing and demonstrated different tubercle configurations in chordwise and spanwise flow conditions on stability margins.

References

[1] F. E. Fish and G. V. Lauder. Passive and active flow control by swimming fishes and mammals. *Annual Review of Fluid Mechanics*, 38:193–224, 2006. doi: 10.1146/annurev.fluid.38.050304.092201.

[2] F. E. Fish, P. W. Weber, M. M. Murray, and L. E. Howle. The tubercles on humpback whales' flippers: application of bio-inspired technology. *Integrative and Comparative Biology*, 51(1):203–213, 2011. doi: 10.1093/icb/icr016.

[3] E. A. van Nierop, S. Alben, and M. P. Brenner. How bumps on whale flippers delay stall: An aerodynamic model. *Physical Review Letters*, 100:054502, 2008. doi: 10.1103/PhysRevLett.100.054502.

[4] H. T. Pedro and M. H. Kobayashi. Numerical study of stall delay on humpback whale flippers. In *46th AIAA Aerospace Sciences Meeting and Exhibit*, Reno, NV, USA, 2008.

[5] P. Watts and F. E. Fish. The influence of passive, leading edge tubercles on wing performance. In *12th International Symposium on Unmanned Untethered Submersible Technology*, Durham, NH, USA, 2001.

[6] J. H. Chen and V. T. Nguyen. The effect of leading edge protubercles on the performance of small aspect ratio foils. In *15th International Symposium on Flow Visualization*, Minsk, Belarus, 2012.

[7] K. L. Hansen, R. M. Kelso, and B. B. Dally. Performance variations of leading-edge tubercles for distinct airfoil profiles. *AIAA Journal*, 49(1):185–194, 2011. doi: 10.2514/1.J050631.

[8] D. S. Miklosovic, M. M. Murray, and L. E. Howle. Experimental evaluation of sinusoidal leading edges. *Journal of Aircraft*, 44(4):1404–1407, 2007. doi: 10.2514/1.30303.

[9] H. Johari, C. Henoch, D. Custodio, and A. Levshin. Effects of leading-edge protuberances on airfoil performance. *AIAA Journal*, 45(11):2634–2642, 2007. doi: 10.2514/1.28497.

[10] S. M. Hasheminejad, H. Mitsudharmadi, and S. H. Winoto. Effect of flat plate leading edge pattern on structure of streamwise vortices generated in its boundary layer. *Journal of Flow Control, Measurement & Visualization*, 2:18–23, 2014. doi: 10.4236/jfcmv.2014.21004.

[11] S. H. Lau, S. Haeri, and J. W. Kim. The effect of wavy leading edges on aerofoil-gust interaction noise. *Journal of Sound and Vibration*, 332(24):6234–6253, 2013. doi: 10.1016/j.jsv.2013.06.031.

[12] M. D. Bolzon, R. M. Kelso, and M. Arjomandi. Tubercles and their applications. *Journal of*

Aerospace Engineering, page 04015013, 2015. doi: 10.1061/(ASCE)AS.1943-5525.0000491.

[13] T. Goruney and D. Rockwell. Flow past a delta wing with a sinusoidal leading edge: near-surface topology and flow structure. *Experiments in Fluids*, 47(2):321–331, 2009. doi: 10.1007/s00348-009-0666-x.

[14] F. E. Fish. Biomimetics: determining engineering opportunities from nature. In *Proc. SPIE 7401, Biomimetics and Bioinspiration, 740109*, 2009. doi: 10.1117/12.824106.

[15] L. E. Howle. Whalepower Wenvor blade: A report on the efficiency of a Whalepower Corp. 5 meter prototype wind turbine blade. Technical report, BelleQuant, LLC, 2009.

[16] P. W. Weber, L. E. Howle, M. M. Murray, and D. S. Miklosovic. Computational evaluation of the performance of lifting surfaces with leading-edge protubercles. *Journal of Aircraft*, 48(2):591–600, 2011. doi: 10.2514/1.C031163.

[17] A. Corsini, G. Delibra, and A. G. Sheard. On the role of leading-edge bumps in the control of stall onset in axial fan blades. *Journal of Fluids Engineering*, 135(8):081104, 2013. doi: 10.1115/1.4024115.

[18] A. K. Malipeddi, N. Mahmoudnejad, and K. A. Hoffmann. Numerical analysis of effects of leading-edge protuberances on aircraft wing performance. *Journal of Aircraft*, 49(5):1336–1344, 2012. doi: 10.2514/1.C031670.

[19] A. Dropkin, D. Custodio, C. W. Henoch, and H. Johari. Computation of flow field around an airfoil with leading-edge protuberances. *Journal of Aircraft*, 49(5):1345–1355, 2012. doi: 10.2514/1.C031675.

[20] A. Skillen, A. Revell, A. Pinelli, U. Piomelli, and J. Favier. Aerodynamic characteristics of finite span wings with leading-edge protuberances. *AIAA Journal*, 53(2):464–472, 2015. doi: 10.2514/1.J053142.

[21] D. S. Miklosovic, M. M. Murray, L. E. Howle, and F. E. Fish. Leading-edge tubercles delay stall on humpback whale (megaptera novaeangliae) flippers. *Physics of Fluids*, 16(5):39–42, 2004. doi: 10.1063/1.1688341.

[22] D. Custodio, C. W. Henoch, and H. Johari. Aerodynamic characteristics of finite span wings with leading-edge protuberances. *AIAA Journal*, 53(7):1878–1893, 2015. doi: 10.2514/1.J053568.

[23] C. A. Ozen and D. Rockwell. Control of vortical structures on a flapping wing via a sinusoidal leading-edge. *Physics of Fluids*, 22(021701), 2010. doi: 10.1063/1.3304539.

[24] K. L. Hansen. *Effect of leading edge tubercles on airfoil performance*. PhD thesis, The University of Adelaide, 2012.

[25] Z Wei, T. H. New, and Y. D. Cui. An experimental study on flow separation control of hydrofoils with leading-edge tubercles at low Reynolds number. *Ocean Engineering*, 108:336–349, 2015.

doi: 10.1016/j.oceaneng.2015.08.004.

[26] T. T. Lim, T. H. New, and S. C. Luo. Scaling of trajectories of elliptic jets in crossflow. *AIAA Journal*, 44(12):3157–3160, 2006. doi: 10.2514/1.25937.

[27] T. H. New and D. Tsovolos. Influence of nozzle sharpness on the flowfields of v-notched nozzle jets. *Physics of Fluids*, 21(8):084107, 1–18, 2012. doi: 10.1063/1.3194306.

[28] T. H. New and D. Tsovolos. On the vortical structures and behaviour of inclined elliptic jets. *European Journal of Mechanics - B/Fluids*, 30(4):437–450, 2011. doi: 10.1016/j.euromechflu.2011.04.006.

[29] J. Bai, C, Y. Y. Lin, S. Y. Lin, and W. C. Wang. Computational fluid dynamics analysis of the vertical axis wind turbine blade with tubercle leading edge. *Journal of Renewable and Sustainable Energy*, 7:033124, 2015. doi: 10.1063/1.4922192.

[30] R. K. Zhang and J. Z. Wu. Aerodynamic characteristics of wind turbine blades with a sinusoidal leading edge. *Wing Energy*, 15:407–424, 2012. doi: 10.1002/we.479.

[31] T. Swanson and K. M. Isaac. Biologically inspired wing leading edge for enhanced wind turbine and aircraft performance. In *Proceedings of the 6th AIAA Theoretical Fluid Mechanics Conference*, Honolulu, HI, USA, 2011. doi: 10.2514/6.2011-3533.

[32] J. Murua, R. Palacios, and J. M. R. Graham. Applications of the unsteady vortex-lattice method in aircraft aeroelasticity and flight dynamics. *Progress in Aerospace Sciences*, 55:46–72, 2012. doi: 10.1016/j.paerosci.2012.06.001.

[33] B. F. Ng, H. Hesse, R. Palacios, J. M. R. Graham, and E. C. Kerrigan. Aeroservoelastic state-space vortex lattice modeling and load alleviation of wind turbine blades. *Wind Energy*, 18(7):1317–1331, 2014. doi: 10.1002/we.1752.

[34] B. F. Ng, R. Palacios, and J. M. R. Graham. Model-based aeroelastic analysis and blade load alleviation of offshore wind turbines. *International Journal of Control*, 2015. doi: 10.1080/00207179.2015.1068456.

[35] J. Katz and A. Plotkin. *Low speed aerodynamics*. Cambridge aerospace series. Cambridge University Press, Cambridge, UK; New York, USA, 2$^{\text{nd}}$ edition, 2001.

[36] B. F. Ng, R. Palacios, J. M. R. Graham, E. C. Kerrigan, and H. Hesse. Aerodynamic load control in HAWT with combined aeroelastic tailoring and trailing-edge flaps. *Wind Energy*, 2015. doi: 10.1002/we.1830.

[37] M. Goland. The flutter of a uniform cantilevered wing. *Journal of Applied Mechanics*, 12(4):A197A208, 1945.

[38] H. Hesse and R. Palacios. Reduced-order aeroelastic models for the dynamics of maneuvering flexible aircraft. *AIAA Journal*, 52(8), 2014. doi: 10.2514/1.J052684.

[39] Z. Wang, P. C. Chen, D. D. Liu, D. T. Mook, and M. J. Patil. Time domain nonlinear aeroelastic analysis for hale wings. In *Proceedings of the 47th AIAA Structures, Structural Dynamics, and Materials Conference*, Newport, Rhode Island, USA, 2006. doi: 10.2514/6.2006-1640.

[40] T. Theodorsen. General theory of aerodynamic instability and the mechanism of flutter. Technical report, NACA 496, 1936.

[41] T. Theodorsen and I. E. Garrick. Mechanism of flutter, a theoretical and experimental investigation of the flutter problem. Technical report, NACA 685, 1938.

[42] Y. C. Fung. *An introduction to the theory of aeroelasticity.* Dover Publications, New York, USA, 1969.

[43] R. L. Bisplinghoff, H. H. Ashley, and L. Robert. *Aeroelasticity.* Addison-Wesley series in mechanics. Addison-Wesley Pub. Co., Cambridge, Mass., USA, 1955.

[44] J. G. Barmby, H. J. Cunningham, and I. E. Garrick. Study of effect of sweep on the flutter of cantilever wings. Technical report, NACA TN 1014, 1951.

[45] W. G. Molyneuz. The flutter of swept and unswept wings with fixed-root conditions. Parts I, II, III. Technical report, Ministry of Supply: Aeronautical Research Council Reports and Memoranda No. 2796, 1950.

[46] A. W. Babister. Flutter and divergence of swept-back and swept-forward wings. Technical report, Ministry of Supply: Aeronautical Research Council Reports and Memoranda No. 2761, 1950.